Original Article

Analysis of electrical characteristics of the four-quadrant converter in high speed train considering pantograph-catenary arcing

Fei Lin[1], Xiaofan Wang[1], Zhongping Yang[1], Hu Sun[1], Wenzheng Liu[1], Ruixiang Hao[1], Jinghai Jiao[2] and Jin Yu[2]

Abstract
Pantograph–catenary disconnection occurs quite frequently in high-speed situations. Pantograph arcing has a significant impact on the contact surfaces and power quality. This article focuses on the effect on the electrical characteristics of the four-quadrant converter of pantograph arcing. An arc model which combines Cassie's arc model with Mayr's arc model is built. This article mainly researches the influence of the pantograph arcing on the four-quadrant converter in different durations. Pantograph arcing leads to voltage pulse in voltage, as well as the harmonics in the current of the alternating current side. At the same time, the direct current voltage decreases when the arc occurs. Therefore, it can ultimately decrease the output torque and increase the torque pulsation of the motor.

Keywords
Pantograph arcing, arc model, four-quadrant converter, direct current voltage, harmonics

Introduction

After the first high-speed railway was put into operation by Japan in 1964, countries around the world began their own development of high-speed railways. During the development of about five decades, the running speed of high-speed railways has increased from 210 to 350 km/h, and the test speed of TGV, developed by France, has held the fastest record of 574.8 km/h since 2007. With the increase of speed, some problems also arise, such as high-speed bogie, aerodynamic performance, and high-speed current collection. This article focuses on the pantograph arcing, which is related to the high-speed current collection quality.

Arcing at the sliding contact between pantograph and overhead contact wire occurs very often, and cannot be fully avoided. It is complex to analyze the effects that these parameters have on arc. Apart from the voltage, current levels, and power factor, the relative motion between the pantograph and overhead contact wire, both in the forward (longitudinal) and lateral (zigzag) directions, and the variable air gap caused by the vertical mechanical oscillations also influences the arc. All of these are time varying. With the rapid development of high-speed railway in China, the speed of many lines has reached 350 km/h. At such a speed, pantograph arcing is more likely to

be generated, which has an enormous influence on current-receiving quality.

It is essential to analyze the impact of pantograph arcing. Pantograph arcing ablates the contact wire, which will shorten the life of the contact wire, or even destroy it. On the other hand, pantograph arcing also distorts the sinusoidal waveform, generates direct current (DC) component, harmonics (including even harmonics and inter harmonics), and generates transients, which cause high-frequency conducted and radiated electromagnetic interference (EMI).

Most previous research has focused more on the EMI/electromagnetic compatibility (EMC) issues from pantograph arcing,[1–6] along with the parameters, these have significant influence on pantograph arcing,[7–13] the electrical characteristics of pantograph arcing,[8,14,15] and so on. Furthermore, some studies have proposed methods used in pantograph to reduce the arcing phenomenon.[11,16] Tang et al.[1] proposed that the high voltage and low current pantograph arcing

[1]School of Electrical Engineering, Beijing Jiaotong University, China
[2]CSR Sifang Co., Ltd., China

Corresponding author:
Fei Lin, School of Electrical Engineering, Beijing Jiaotong University, No. 3 Shangyuancun, Haidian District, Beijing 100044, People's Republic of China.
Email: flin@bjtu.edu.cn

would generate the electric field which radiates on the surface of coaxial-cables, and differential mode voltages acting on communication interface will form at once due to the transfer impedance. When the voltages combine into a generated signal, incorrect actions of the Cab Integrated Radio may occur, and the system may even be destroyed. Tellini et al.[3] analyzed the influence of the capacitor paralleled with pantograph arcing in Italy's DC traction power supply system. Earlier studies[8,10,13] presented an experimental analysis to understand the influence of different parameters, including the relative speed of the sliding contact electrode, supply current, supply voltage, reactive load, materials and shape of electrodes, and so on. Wang et al.[14] proposed the electrical characteristics of the pantograph arcing. Pantograph arcing voltage and current are polarity dependent phenomena. The voltage and current waveform is asymmetrical at pantograph arc burning, which leads to a DC component and harmonics component in the system. Some work also focus on the electrical erosion of the arc.[15]

The high-speed current collection quality has a great influence on the traction drive system, due to structural relationship between the catenary and transformer. The traction drive system consists of a traction transformer, four-quadrant converter, inverter, and motor, which offer tractive force to the high-speed train. When the current collection quality becomes poor, the tractive force would drop significantly. Additionally, the overshoot of arc voltage during the burning of arc has a great effect on the alternating current (AC) and DC voltage of the four-quadrant converter. This may result in the effect of tractive force, or even damage to the IGBT. Meanwhile, some studies have focused on how the pantograph arcing affects the traction drive system, especially the four-quadrant converter. Wang et al.[17] discussed how the pantograph arcing affects the transient inductance of the Main Transformer. The present article discusses the impact of the pantograph arcing on a four-quadrant converter by establishing the dynamical traction drive system model, while considering the effects of pantograph arcing.

Arc model

Principles of the arc model

During circuit breaker operation, the gap between electrodes changes rapidly from a conductive plasma to an insulating gas. The electrical arc performance during this short period of time is dependent on the thermal balance, thermal inertia, and thermal ionization in the plasma column.[18] There are two types of arc models which are widely used in the analysis of the arc phenomenon. The first type is built to analyze the internal characteristics of the arc, which can be used in the EMI analysis of the pantograph arcing.[19,20] The second, known as the black box model, is used to simulate the external voltage and current characteristics of the arc.[21–24] Although this approach does not offer much internal characteristics of the arc, it is relatively simple. When extensive test data are available, the use of this type of arc model is feasible.[18,25] The present article focuses on the electrical impact of the arc, thus the second type of arc model is taken into account.

The aim of black box models is to use voltage and current traces from the test, together with a given differential equation, to deduce a mathematical model for the arc. Most of the published work regarding black box models is based on the well-known Cassie and Mayr models, which provide a qualitative description of the arc in the high-current and low-current regions, respectively.[25–27] The Cassie model regards the arc as a cylindrical plasma, while the diameter varies with the change of current, and the energy dissipation of the arc is directly related to the cross-sectional area.[28] The Mayr model is similar to the Cassie model in some aspects, such as regarding the arc as a constant diameter cylindrical plasma. The power dissipation of the Mayr model is considered through thermal conduction and thermal radiation simultaneously. The final expression of the Cassie and Mayr model is as follows:

$$\frac{1}{g_C}\frac{dg_C}{dt} = \frac{1}{\tau}\left(\frac{u^2}{E_0^2} - 1\right) \tag{1}$$

$$\frac{1}{g_M}\frac{dg_M}{dt} = \frac{1}{\tau}\left(\frac{ui}{P_0} - 1\right) \tag{2}$$

where g_M and g_C are the Mayr and Cassie arc conductances, respectively; τ expresses the arc's time constant; P_0 is the cooling power in the Mayr arc model; E_0 is the transient static arc voltage of the Cassie arc model; and u is the instantaneous voltage of the arc, while i is the instantaneous current of the arc.

Based on the traditional Mayr and Cassie arc models, this article uses a novel arc model, which is combined with the Mayr and Cassie arc models. Dai[29] and Suh et al.[30] have determined a transition function considering the stability of the arc, but it cannot describe the low-current state of the arc due to the range of the function. To describe the characteristics of the arc, the author proposes the transition function $\sigma(i)$, which changes with the current. The Mayr and Cassie arc models can be coupled by the following equation:

$$g_{arc} = (1 - \sigma(i))g_C + \sigma(i)g_M \tag{3}$$

As Cassie's equation shows good results for larger currents, while Mayr's is better for the low current section, the $\sigma(i)$ is a monotone function varying from 0 to 1. Through comparing the characteristics of equation (3), the transition function is finally determined as follows:

$$\sigma(i) = \exp\left(-\frac{i^n}{I_0^n}\right) \qquad (4)$$

where i represents the instantaneous current of the arc; and I_0 represents the current constant. The parameter n can be determined according to experimental and simulated results to correct the arc model.

Considering all of these influencing factors, the following arc model is built:

$$\left.\begin{aligned}
g_{arc} &= (1 - \sigma(i))\,g_C + \sigma(i)\,g_M \\
\frac{1}{g_M}\frac{dg_M}{dt} &= \frac{1}{\tau}\left(\frac{ui}{P_o} - 1\right) \\
\frac{1}{g_C}\frac{dg_C}{dt} &= \frac{1}{\tau}\left(\frac{u^2}{E_o^2} - 1\right)
\end{aligned}\right\} \qquad (5)$$

However, the final arc model has yet to be built, as there are also some parameters, which are not yet determined. P_0 is the cooling power of the arc. When the input power of the arc ui is larger than P_0, temperature of the arc rises; otherwise, the temperature drops. E_0 is the transient static arc voltage, which is irrelevant with the current i.

Parameter determination of the arc model

As discussed before, there are some parameters which must be selected to ensure that the arc model can reflect the characteristics of the pantograph arcing, such as the cooling power of Mayr arc model P_0, transient static arc voltage of Cassie arc model E_0, time constant τ, and current constant of transition function I_0.

The following experimental apparatus, as shown in Figure 1, has been established to provide the test data to confirm the parameters of the arc model.

The overhead contact wire is fixed in a groove around the outer edge of the large wheel. One side of the axle of the wheel is connected to the motor, of which the rotating speed can be controlled. The other side is connected to a carbon brush collector to ensure the stability of current collection.

The pantograph consists of a pantograph slide plate, spring support, and power unit, which can provide vertical oscillations to the pantograph. Another smaller motor linearly drives the carriage back and forth, so that it can guarantee the pantograph moves in a zigzag motion.

The experimental apparatus can provide the external voltage and current characteristics, which can be used in rectifying the arc model. The experimental and
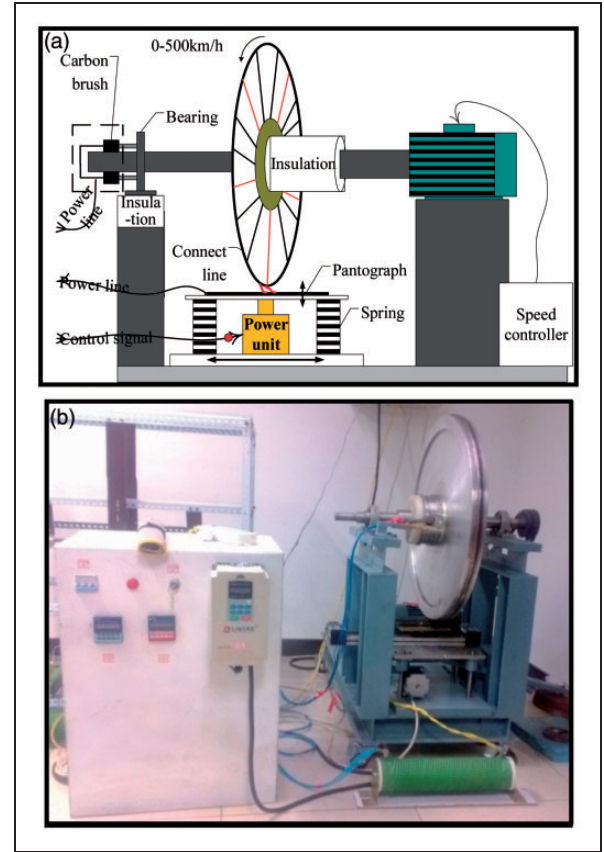

Figure 1. (a) Schematic diagram of the experimental apparatus and (b) photo of the experimental apparatus.

simulated waveforms are shown in Figure 2, and the parameters of the arc are determined as shown in Table 1.

Analysis of four-quadrant converter considering pantograph arcing

The traction drive system is the backbone system of the train and can transfer electrical energy to the mechanical energy driving the train. The traction drive system of the high-speed train is made up of the current collecting system, traction transformer, traction converter and motors, and so on. The circuit schematic of the system is shown in Figure 3.

This article focuses on the influence of pantograph arcing on the four-quadrant converter. The main function of the four-quadrant converter is to change the AC of the transformer's secondary circuit to DC, which can be used in the inverter. The DC voltage has great effect on the torque of the motor, which decides the running status of the train.

Circuit of the four-quadrant converter

The structure of the single-phase four-quadrant converter is the same as the full bridge phase-controlled rectifier, in which the switching devices consist
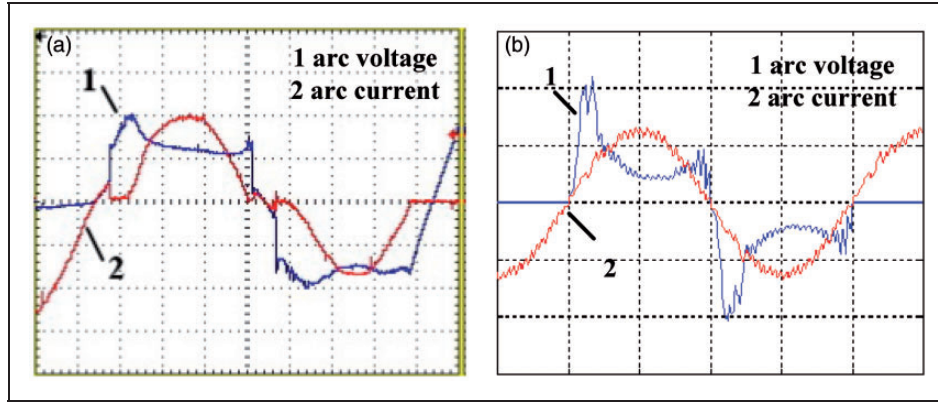
Figure 2. Correction of the pantograph arcing model: (a) Experimental waveforms and (b) simulated waveforms.

Table 1. Determined parameters of arc model.

Undetermined parameter	Meaning of the parameter	Value of the parameter
P_0	Cooling power of Mayr arc model	10^5
E_0	Transient static arc voltage of Cassie arc model	3×10^4
τ	Time constant of arc	3.6×10^{-4}
I_0	Current constant of transition function	10^2

of full-controlled devices paralleled with diode. The schematic circuit diagram is shown in Figure 4, where R_N is the leakage resistance of the traction transformer's secondary circuit, L_N is the inductance of the AC side, C_d is the capacitance of the DC side, R_L is the load resistance of the four-quadrant converter, u_N is the input voltage of the AC side, i_N is the input current of the AC side, u_{ab} is the modulating voltage of the PWM, and u_d is the output current of the DC side.

There are two states of the four-quadrant converter. In the first state, the current flows through T_1 and T_4, while the other flows through T_2 and T_3, ignoring the influence of the dead zone. In period k, we assume the duty ratio of pulse on T_1 and T_4 is d_k, thus the duty ratio of pulse on T_3 and T_2 is 1-d_k. According to the Kirchhoff's current law and Kirchhoff's voltage law, the state equation is as shown below:

$$
\begin{bmatrix} L_N \dfrac{di_N}{dt} \\ C_d \dfrac{du_d}{dt} \end{bmatrix} = \begin{bmatrix} -R_N & 1-2d_k \\ 2d_k-1 & -\dfrac{1}{R_L} \end{bmatrix} \begin{bmatrix} i_N \\ u_d \end{bmatrix} + \begin{bmatrix} u_N \\ 0 \end{bmatrix}
\tag{6}
$$

There are intermediate parameters d_k, which can be used instead of the following equation, where k is the

number of the period:

$$
d_k = \frac{\int_{(k-1)T_s}^{kT_s} u_{ab} dt}{U_d \cdot T_s}
\tag{7}
$$

An equation is also needed to associate the u_{ab} and i_N. This equation can be calculated in the control strategy of the four-quadrant converter.

Control strategy of the four-quadrant converter

To determine the modulating voltage u_{ab}, the double closed-loop control strategy is used, which consists of an outer voltage loop and inner current loop. The control block diagram is shown in Figure 5, where P_d is the root mean square (RMS) value of DC power and u_L is the inductance voltage of the AC side. We then calculate the I_{N1}, which represents the original directive value of DC current through the difference of U_d* and u_d. To promote the dynamic response of the control strategy, I_N*, which represents the final reference value of the DC current, is calculated through a compensator. Then, the u_{ab} is determined according to the difference of I_N* and I_N.

The mathematic equation of the control strategy is shown as follows:

$$
\left.\begin{array}{l} I_{N1} = k_p(U_d^* - u_d) + \dfrac{1}{T_i} \int (U_d^* - u_d)\,dt \\ I_{N2} = \dfrac{P_d}{U_N} \\ I_N^* = I_{N1} + I_{N2} \\ u_{ab} = u_N - \omega_m L_N I_N^* \cos\omega_m t - G_2[I_N^* \sin\omega_m t - i_N] \end{array}\right\}
\tag{8}
$$

where k_p and T_i are the parameters of the PI controller, G_2 is the proportionality factor, U_d^* is the reference value of DC voltage, and U_N is the RMS value of the AC voltage.

Therefore, the relationship is built from equation (8), which can be input into equation (7), so that the equation of the four-quadrant can finally be established, which is the same as equation (6), where the d_k is expressed in the following form equation (9).
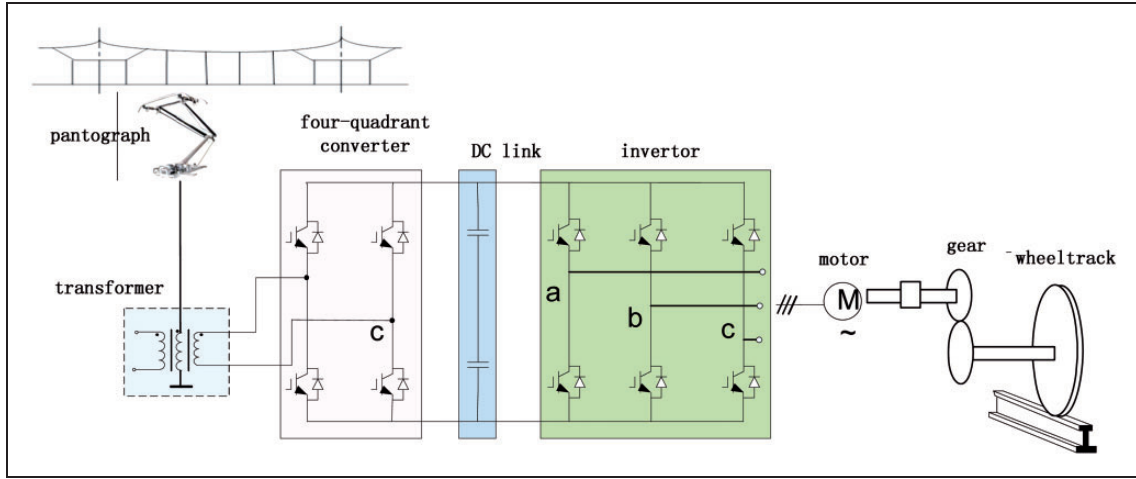
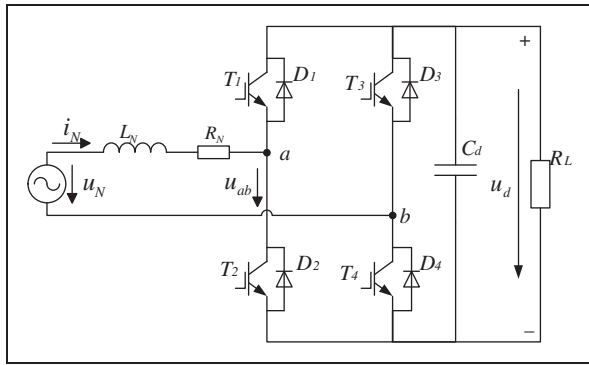**Figure 3.** Schematic diagram of the traction drive system.

Figure 4. Schematic diagram of the four-quadrant converter.

Model combining four-quadrant converter and pantograph arcing

Considering the effect of pantograph arcing, the following equation can be obtained, if regarding the pantograph arcing as a model of which the current is varied when the voltage is changing.

$$
d_k = \frac{\left\{\begin{array}{c} \int_{(k-1)T_s}^{kT_s} \left[u_N - \omega_m L_N \left(k_p (U_d^* - U_d) \right. \right. \\ + \frac{1}{T_i} \int (U_d^* - U_d) \mathrm{d}t + \frac{I_d U_d}{U_N} \right) \\ \left. \times \cos \omega_m t - G_2 (I_N^* \sin \omega_m t - i_N) \mathrm{d}t \right] \end{array}\right\}}{U_d \cdot T_s}
$$

(9)

$$
\left. \begin{array}{l} u_s = \dfrac{i_s}{g_{arc}} + K u_N \\ i_s = K i_N \end{array} \right\}
$$

(10)

In equation (10), K is the transformer ratio.

We then combine the state equation of the four-quadrant converter with the equation considering the effect of pantograph arcing. Then, the following equations can be worked out.

$$
\begin{bmatrix} L_N \dfrac{di_N}{dt} \\ C_d \dfrac{du_d}{dt} \end{bmatrix} = \begin{bmatrix} -R_N & 1 - 2d_k - \dfrac{1}{g_{arc}} \\ 2d_k - 1 & -\dfrac{1}{R_L} \end{bmatrix} \\ \times \begin{bmatrix} \dfrac{i_s}{K} \\ u_d \end{bmatrix} + \begin{bmatrix} \dfrac{u_s}{K} \\ 0 \end{bmatrix}
$$

(11)

The d_k can be calculated in equation (9), while the g_{arc} is shown in equation (5).

The performance of the four-quadrant converter can be affected greatly in such a tightly coupled system. It is crucial to explore the effects of pantograph arcing on the four-quadrant converter.

Results and analysis

According to the previous analysis of four-quadrant converter considering pantograph arcing, we then build the simulation model of the four-quadrant converter considering pantograph arcing, which is shown in Figures 6 and 7. To analyze the effect of pantograph arcing on the four-quadrant converter, the resistance load (1.2 MW) is connected in series in the terminal of the converter. This article then discusses the effects of the arc in terms of the following aspects: duration of arc and initial phase of arc.

This Simulink model is based on the parameters of the Chinese high speed train CRH2. The parameters used in the simulation are listed in Table 2.

Results without considering pantograph arc

Using the simulation model introduced in the previous section, the results of the four-quadrant converter are obtained while the pantograph is tightly connected with the catenary. The DC voltage, AC voltage, and AC current of the simulation are shown in Figure 8.
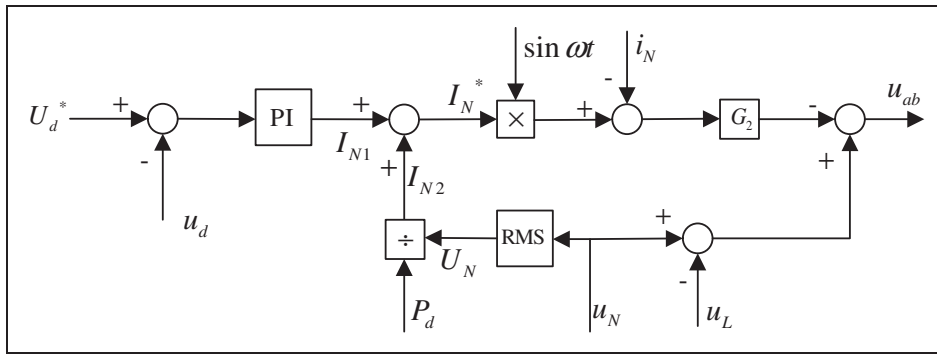
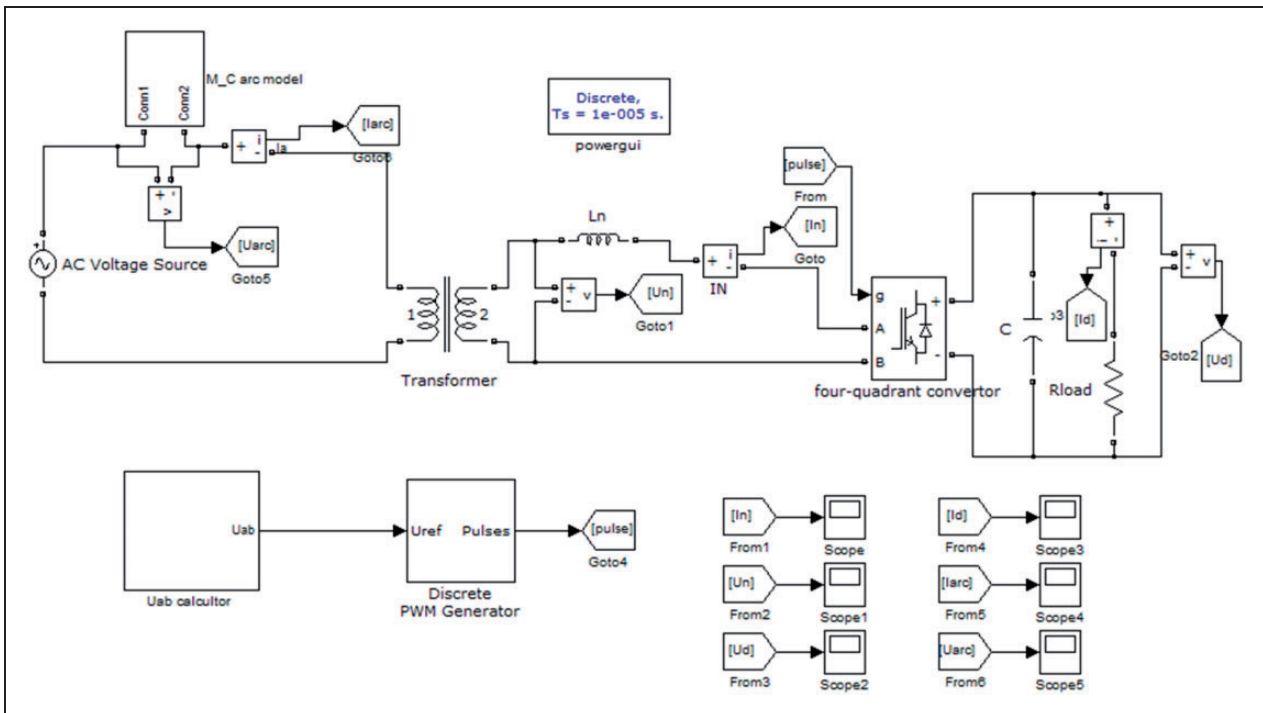**Figure 5.** Control block diagram of the control strategy.

Figure 6. Simulink model of the four-quadrant converter considering the pantograph arcing.
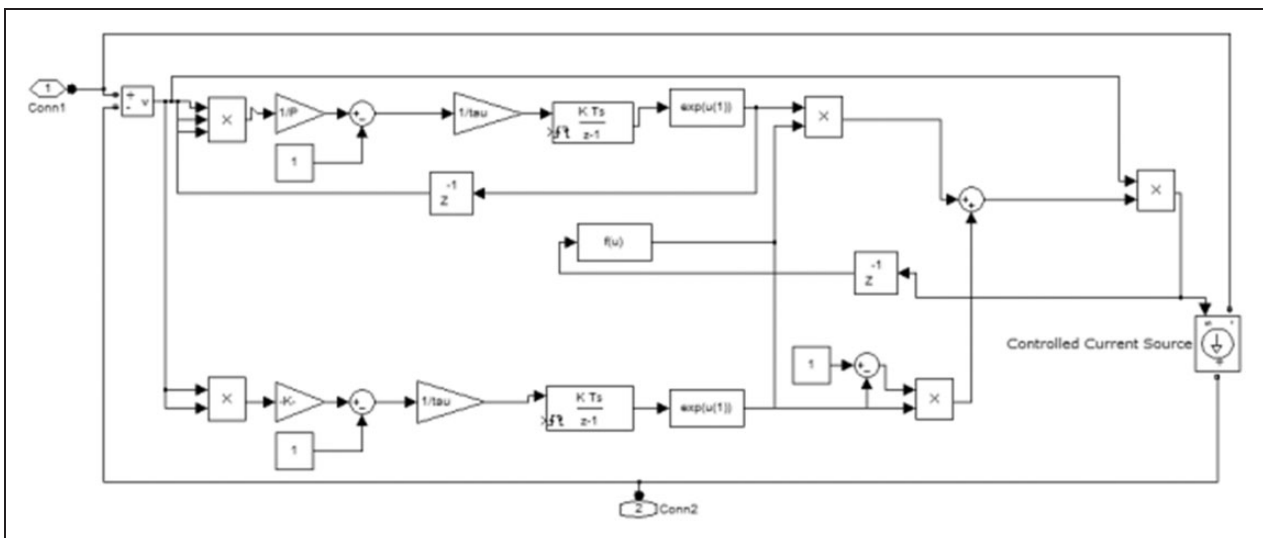

Figure 7. Simulink model of the pantograph arcing.

It can be seen from Figure 8 that the fluctuation of the DC voltage is about 170 V when the converter is used in normal operation state. There is no obvious distortion in the secondary winding voltage and current. The peak voltage of the secondary winding of the transformer is 2121 V, which satisfies the requirements. The average voltage of the DC voltage is 3100 V, which is equal to the directive value of the DC voltage.

The results of the Fast Fourier Transform (FFT) analysis of the AC current are shown in Figure 9.

From Figure 9, it can be easily concluded that the harmonics of the four-quadrant converter mainly contains even times the switch frequency; for instance, 2500 Hz, 5000 Hz, and so on, while the amplitude of the harmonics decreases with the increase of the frequency.

Influence of duration of arc

Because of the characteristics of the AC arc, the arc quenches when the current passes through the zero. It

Table 2. Parameters of the four-quadrant converter.

Parameter	Meaning of the parameter	Value
U_{s1}	Voltage of catenary	25 kV
U_{s2}	Voltage of secondary winding of transformer	1500 V
U_d	Voltage of DC voltage	3100 V
R_N	Leakage resistance of traction transformer's secondary winding	0.001 Ω
L_N	Inductance of AC side	2.195e-3 H
C_d	Capacitor of the DC side	7e-3 F
R_{load}	Equal resistance of load	8.94 Ω
f_s	Frequency of switch	1250 Hz
f	Frequency of fundamental wave	50 Hz

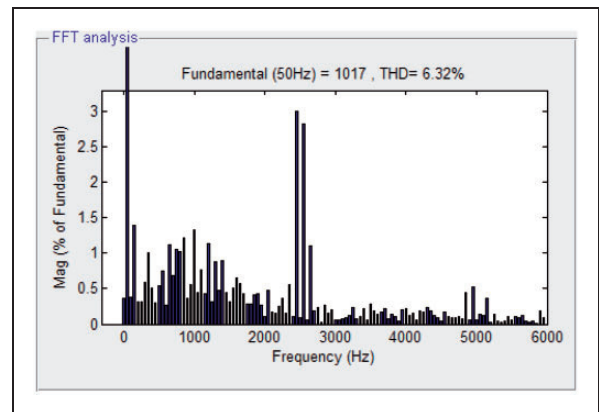DC: direct current; AC: alternating current.

Figure 9. FFT analysis of the AC current.
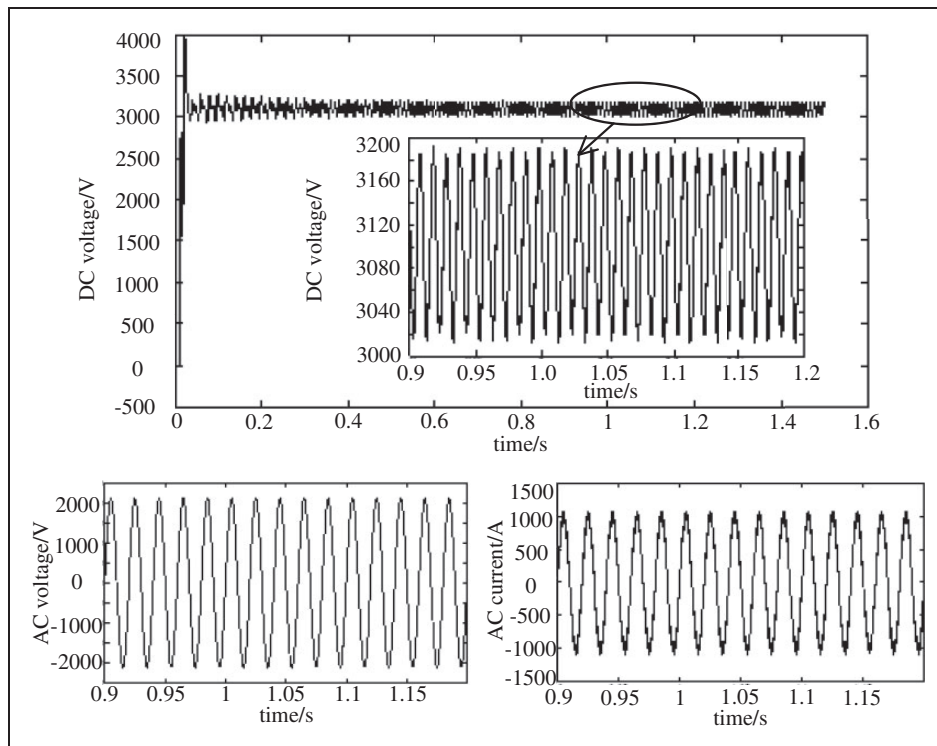FFT: Fast Fourier Transform; AC: alternating current.

Figure 8. Simulated waveforms of DC voltage, AC voltage, and AC current.
DC: direct current; AC: alternating current.

is not necessary to analyze the duration of the arc beyond the half period of the fundamental wave, due to the simple repeat in each half period. We select the following four durations of arc: the arc lasts for 0.125, 0.25, 0.375, and 0.5 periods of the fundamental wave. To analyze the harmonics of the arc, each situation of four durations of the arc is repeated for two periods. Table 3 shows the duration of each simulation.

Table 3. Theduration of each simulation.

Serial number	Duration of arc	Start time (s)–stop time (s)
1	0.125	1.0000–1.0025 1.0200–1.0225
		1.0100–1.0125 1.0300–1.0325
2	0.25	1.0000–1.0050 1.0200–1.0250
		1.0100–1.0150 1.0300–1.0350
3	0.375	1.0000–1.0075 1.0200–1.0275
		1.0100–1.0175 1.0300–1.0375
4	0.5	1.0000–1.0400

Effect of duration of arc on voltage

From the previous analysis, it can be concluded that the pantograph arc has a great effect on the voltage, especially when the overshoot of the arc voltage occurs. Figure 10 is the AC voltage waveform in different durations of arc.

In Figure 10(a) to (d), the voltage pulse occurs at the same time when the pantograph arc begins, and the AC voltage distorts severely at this time. Aside from the first and third times, the voltage pulse is negative whereas the others are opposite. This is closely connected with the characteristics of the arc. When the arc begins, there is an overshoot of voltage. When the arc occurs, there is a high voltage which must be beyond the breakdown voltage of the air between the photograph and catenary. When the photograph arcing is lit, the voltage will hold on at a small value which can maintain the arc. If we ignore the voltage drop of the high voltage equipment at the roof of the carriage, the voltage of the transformer on the primary side is equal to the voltage of the catenary minus the arc voltage. The circuit before the four-quadrant converts does not have the capacitor, thus
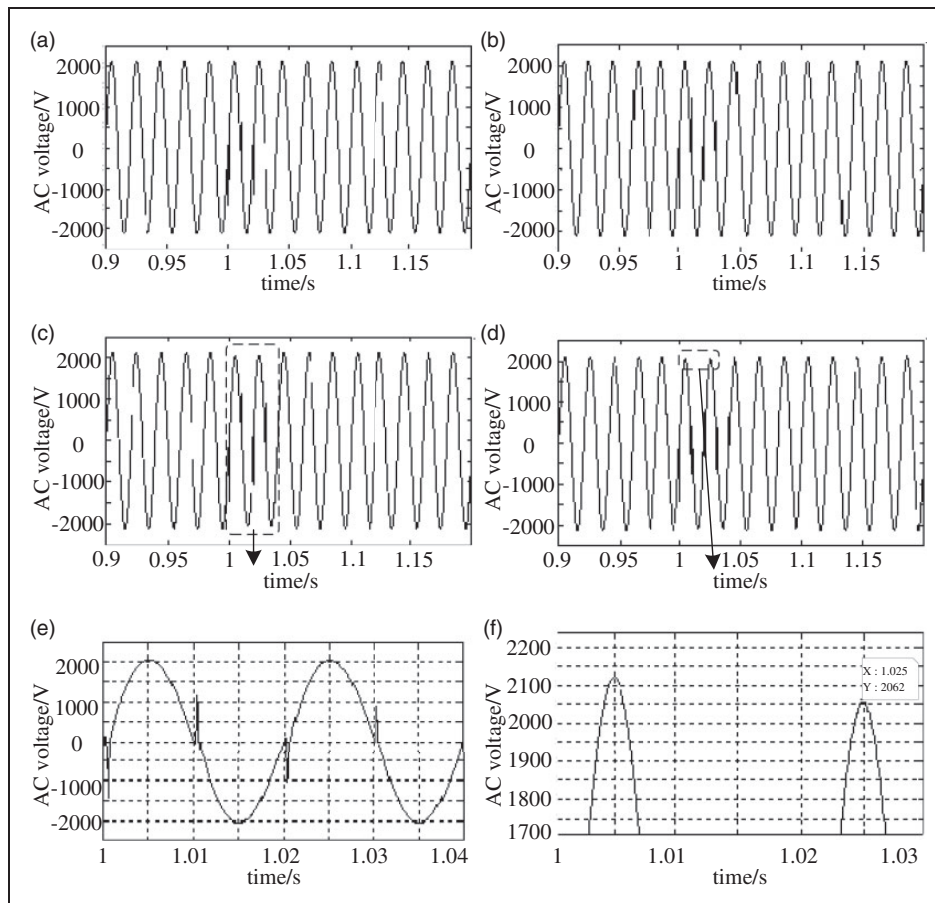

Figure 10. AC voltage: The duration is (a) 0.125 period; (b) the duration is 0.25 period; (c) the duration is 0.375 period; (d) the duration is 0.5 period; (e) the partial enlarged drawing of 0.375 period; (f) the partial enlarged drawing of 0.5 period.
AC: alternating current.

the overvoltage transmitted through the transformer affects the AC voltage. Meanwhile, when the overvoltage of the pantograph arcing occurs in the positive half period, the AC side voltage occurs in the negative half period. When the duration of the arc is 0.375 period, the value of the pulse amplitude is about 1000 V, which is approximately equivalent to 50% of the value of peak voltage, as shown in Figure 10(e).

At the same time, the duration of pantograph arcing can also lead to a decrease of the AC voltage. Perhaps, this is not obvious in Figures 10(a) to (d), whereas Figure 10(f), which is the partial enlarged image of Figure 10(d), clearly exhibits this phenomenon. In Table 4, the decrease value when the AC voltage is at the peak value is concluded. The decrease of voltage is about 58 V when the duration of arc is 0.375 or 0.5 period, while there is no voltage decrease under the other conditions.

Although the peak value of AC voltage has not changed in the duration of 0.125 and 0.25 period, the voltage decrease also exists. When the duration of the arc includes the AC peak point, the peak value decreases slightly. The decrease value is affected

Table 4. Voltage decrease of AC side with different durations.

Duration of arc	Voltage decrease of AC peak value
0.125 period	0 V
0.25 period	0 V
0.375 period	58 V
0.5 period	58 V

AC: alternating current.

by the arc voltage in constant proportion. However, when the duration of the arc does not include the AC peak point, the peak value will be the same.

When the arc is burning stably, the volt-ampere characteristic of the arc is just like a resistor. The voltage decreasing on both the AC and DC sides is inevitable. The value of voltage decrease is affected by the duration of the arc, the length of the arc column, and the volt-ampere characters of the arc. The change of the length of the arc column and the character of the arc require a more accurate arc model. When the length of the arc is constant, the voltage drop of the AC voltage is only determined by the volt-ampere characters of the arc.

At the same time, the DC voltage is also affected by the pantograph arcing. Because of the role of the capacitor, the DC voltage has not overshot the voltage during the arc. However, the voltage decrease is more obvious. Figure 11 is the partial enlarged image of the DC voltage, which indicates how the DC voltage is affected by the pantograph arcing.

In Figure 11, the point of the voltage decrease is emphasized by the small circle. It is apparent that the DC voltage valley value at the same point is about 1.0125 s. However, the decrease voltage is the not same as the increase the duration of the arc. Figure 12 shows the value of voltage decrease with different durations of the arc, which indicates the different effects.

From Figure 12, it is significant that the when the pantograph arcing occurs, the DC voltage decreases by different degrees. The decrease value increases with the increase of the duration of arc. Meanwhile, the decrease of the valley value is slightly larger than the peak. It is in accordance with the characteristics
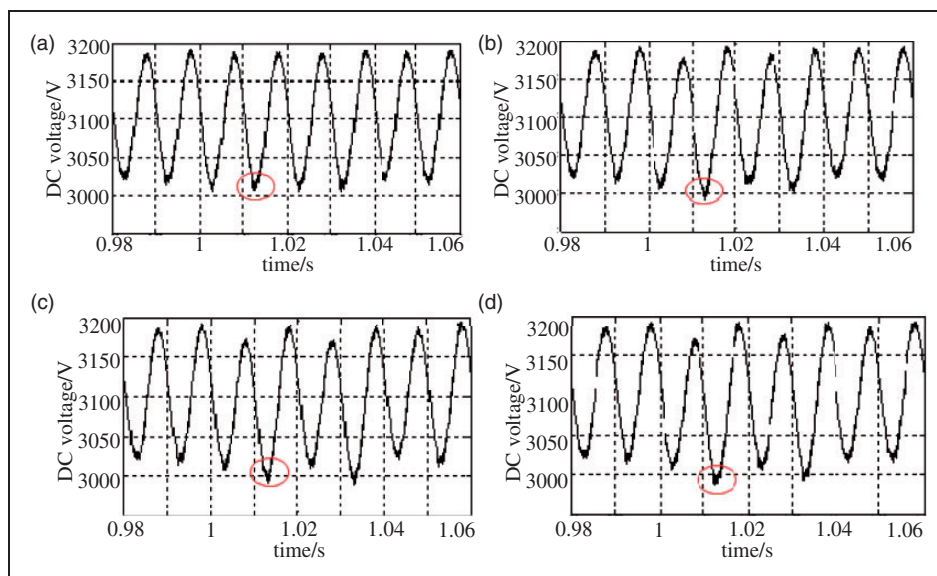

Figure 11. DC voltage: (a) The duration is 0.125 period; (b) the duration is 0.25 period; (c) the duration is 0.375 period; (d) the duration is 0.5 period.
DC: direct current.

of the arc that the arc has a DC component. Because of the different materials of the pantograph and catenary, the DC component exists in the arc. The DC component has a great influence on the transformer. It also affects the DC voltage of the output of the four-quadrant converter.

DC voltage is a crucial parameter of the traction drive system, which includes the output of the four-quadrant converter as well as the input of the inverter. The DC voltage decrease increases with the increase of the duration of the arc. When the arc persists for a period of the fundamental wave, the voltage decrease is about 30 V, which is about 1% of the DC voltage. Meanwhile, the voltage decrease of the valley is larger than the voltage decrease of the peak. The voltage decrease of the DC side can lead to the decrease of the traction pull, which restricts the speed improvements of the high-speed train.

Influence of the duration of arc on current

However, the current on both the AC and DC sides does not exhibit a visual phenomenon in the
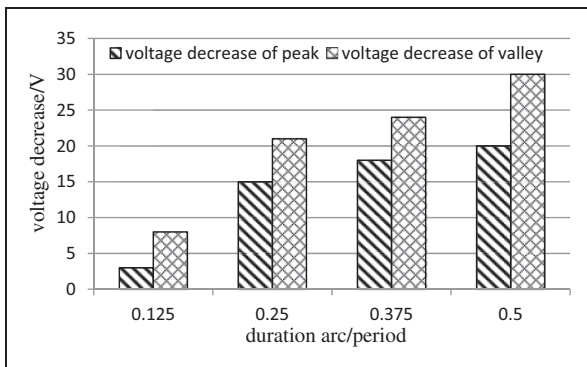

Figure 12. Statistics of the DC voltage decrease.
DC: direct current.

waveform, while the values of the fundamental wave and the harmonics have increased slightly. Figure 13 is the FFT analysis of the AC current with both no arc and in two periods of the arc. It is easily concluded that the arc leads to harmonics mainly in the frequency below 500 Hz.

From Figure 13, it can be seen that the pantograph arc has a great effect on the AC current harmonics, DC component, 100 Hz and 150 Hz components, which all increase significantly. Therefore, it is necessary to research the influence of the arc's duration on the AC current harmonics.

The simulation is also proceeding in the previous four conditions, in which the pantograph lasts for 0.125, 0.25, 0.375, and 0.5 period. Figure 14 is the harmonics analysis results of the different conditions.

It can be easily concluded that the RMS value of the fundamental current of the AC side is about 1050 A, and that it increases slowly with the increase of the arc duration. At the same time, the DC component and harmonic below the 150 Hz are greatly affected by the period of the arc. However, as for the frequencies beyond 150 Hz, there are no significant rules with the increase of the arc's duration; for example, the 200 Hz harmonic current reaches the maximum when the duration of arc is 0.375 period, whereas the 450 Hz reaches when the arc's duration is 0.25 period with all four of the conditions. Table 5 shows the calculated values of the different durations of the arc with different frequencies below 200 Hz.

Table 5 shows that the DC component increases greatly from 3.6 to 26.3 A with the duration from 0.125 to 0.5 period, and that the 100 Hz harmonic increases from 10.3 to 26.3 A. The RMS current of the 150 Hz changed slightly while the arc's duration changed. This also matches with the characteristics of the pantograph arcing. The voltage decrease in the arc is not symmetric in either of the half cycles of the power supply. When the catenary is the positive electrode, the
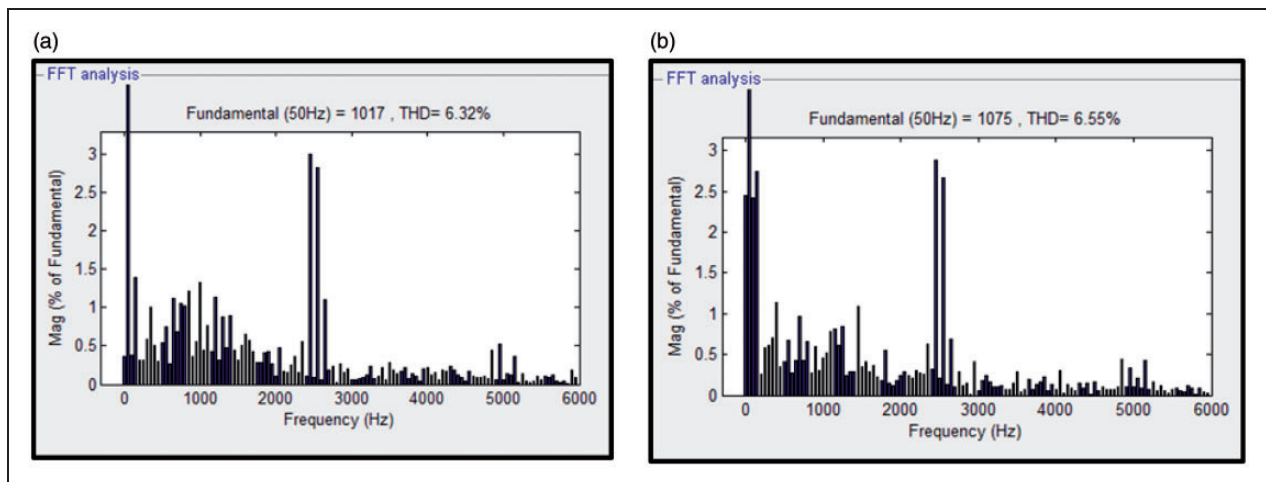

Figure 13. The FFT analysis of the AC current: (a) With no arc and (b) with two periods of arc.
FFT: Fast Fourier Transform; AC: alternating current.

voltage decrease is low, whereas the opposite is large. Therefore, the DC component is generated in the AC supply, which can drive the DC current to cross the traction drive system. At the same time, the DC components also inject into the AC supply network. The DC component in the AC supply high-speed train system can lead to many consequences.

Above all, the periods of the pantograph have distinct effects on the four-quadrant converter, in terms of both the voltage and current. The main effects of the pantograph arcing's duration on the voltage are the overshoot of the AC voltage, and the voltage decrease of the AC and DC sides. At the same time, the overshoot of AC voltage occurs at the point where the arc begins. Meanwhile, the voltage decrease of the AC peak voltage occurs when the duration of the arc includes the point where the AC voltage is at peak value, and the DC voltage decrease is more significant, increasing with the increase of the arc duration. The effects of arc duration on current mainly occur in the DC component and harmonics. When the frequency is below 150 Hz, the RMS values of the harmonics and DC component increase with the increase of the duration.
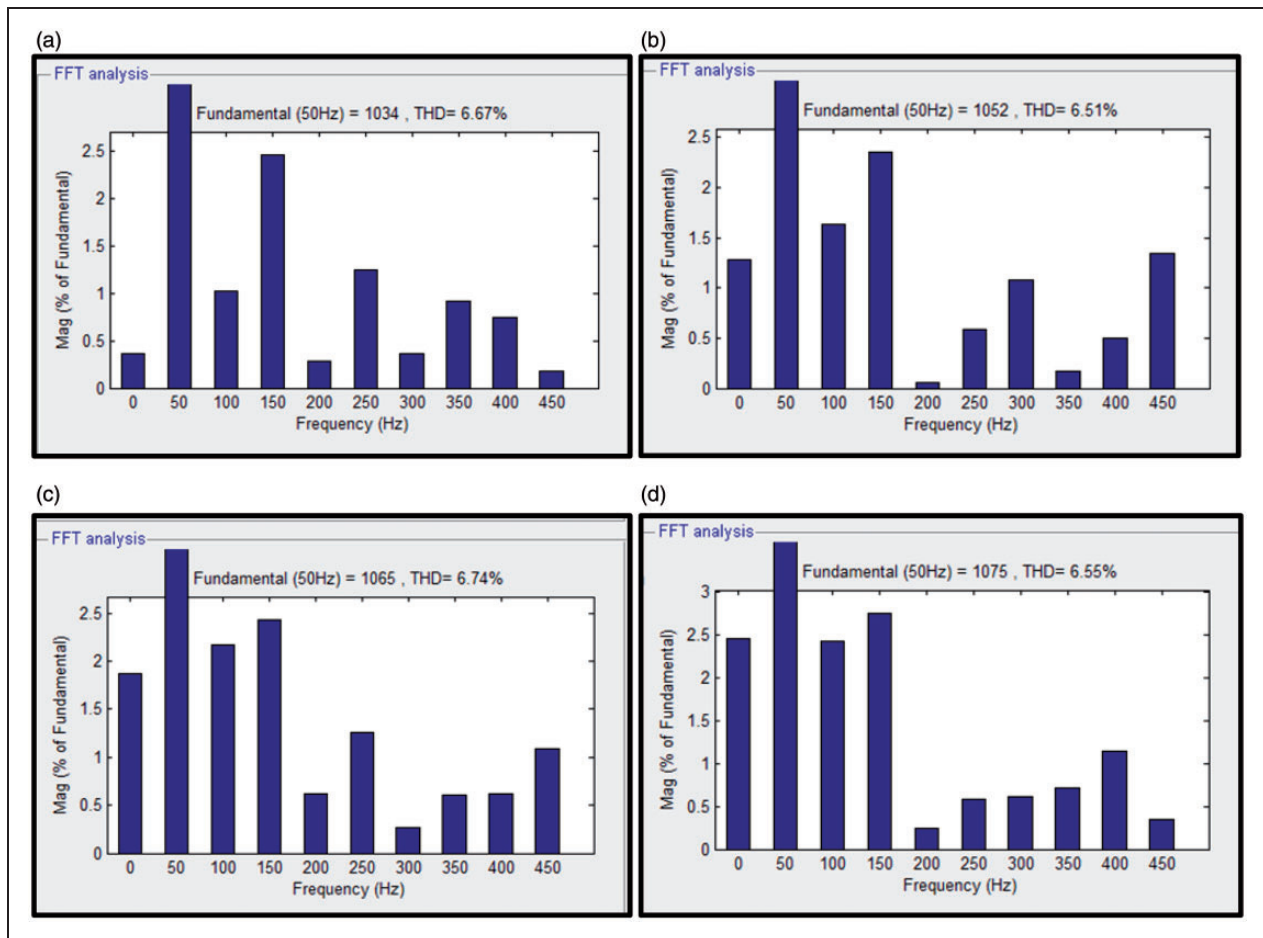

Figure 14. The FFT analysis of different duration: (a) The duration is 0.125 period; (b) the duration is 0.25 period; (c) the duration is 0.375 period; (d) the duration is 0.5 period.
FFT: Fast Fourier Transform.

Table 5. RMS current with different durations of arc.

Duration of arc	RMS current of 50 Hz	RMS current of DC	RMS current of 100 Hz	RMS current of 150 Hz
0.125 period	1034 A	3.6 A	10.3 A	24.8 A
0.25 period	1052 A	13.1 A	16.8 A	25.2 A
0.375 period	1065 A	19.7 A	23.4 A	25.6 A
0.5 period	1075 A	26.3 A	26.3 A	29.6 A

DC: direct current; RMS: root mean square.

Conclusion

In this article, the experimental apparatus is established to rectify the arc model. Then, the arc model is built to analyze the effects of pantograph arcing on the four-quadrant converter. Finally, the model of the four-quadrant converter considering the arc is built. The analysis is carried forward in terms of two aspects: the voltage influence of the duration of the arc, and the current influence of the duration of the arc. The following conclusions are obtained:

1. The effect of the AC voltage is the overshoot voltage when the arc is beginning, whereas the DC voltage presents the relationship between the voltage decrease and the duration of the arc. The voltage decrease increases greatly with the increase of the duration.
2. The duration of the arc affects the AC current on the DC component and the harmonics. The DC component and the harmonic current below 150 Hz increase with the increase of the duration.

However, the model built in the article is simpler than the real traction drive system. To analyze the effects of arc on converter, the inverter and motor have been ignored in this article. The effects of pantograph arcing on the entire traction drive system should be concluded in future research.

Declaration of Conflicting Interests

The author(s) declared no potential conflicts of interest with respect to the research, authorship, and/or publication of this article.

Funding

References

1. Tang ZM, Zhu F, Luo XR, et al. Analysis of EMI on Cab Integrated Radio communication equipment. In: *IEEE Cross Strait Quad-Regional Radio Science and Wireless Technology Conference (CSQRWC)*, Harbin, People's Republic of China, vol. 1, July 2011, pp.281–284. USA: IEEE.
2. Guodong W. Characteristics of radio frequency interference from pantograph arcing in car of traction stock. In: *IEEE 3rd International Symposium on Microwave, Antenna, Propagation and EMC Technologies for Wireless Communications*, Beijing, People's Republic of China, October 2009, pp.207–210. USA: IEEE.
3. Tellini B, Macucci M, Giannetti R, et al. Line-pantograph EMI in railway systems. *IEEE Instrum Meas Mag* 2001; 4: 10–13.
4. Mariscotti A, Marrese A, Pasquino N, et al. Time and frequency characterization of radiated disturbance in telecommunication bands due to pantograph arcing. *Measurement* 2013; 46: 4342–4352.
5. Fridhi H, Deniau V, Ghys JP, et al. Analysis of the coupling path between transient EM interferences produced by the catenary-pantograph contact and on-board railway communication antennas. In: *IEEE 2013 International Conference on Electromagnetics in Advanced Applications (ICEAA)*, Torino, Italy, September 2013, pp.587–590. USA: IEEE.
6. Midya S, Bormann D, Mazloom Z, et al. Conducted and radiated emission from pantograph arcing in AC traction system. In: *IEEE Power & Energy Society General Meeting (PES'09)*, Calgary, Canada, July 2009, pp.1–8. USA: IEEE.
7. Midya S, Bormann D, Schütte T, et al. Pantograph arcing in electrified railways—Mechanism and influence of various parameters—Part I: With DC traction power supply. *IEEE Trans Power Deliver* 2009; 24: 1931–1939.
8. Midya S, Bormann D, Schütte T, et al. Pantograph arcing in electrified railways—Mechanism and influence of various parameters—Part II: With AC traction power supply. *IEEE Trans Power Deliver* 2009; 24: 1940–1950.
9. Bormann D, Midya S and Thottappillil R. DC components in pantograph arcing: mechanisms and influence of various parameters. In: *IEEE 18th International Zurich Symposium on Electromagnetic Compatibility (EMC Zurich)*, Munich, Germany, September 2007, pp.369–372. USA: IEEE.
10. Midya S, Bormann D, Larsson A, et al. Understanding pantograph arcing in electrified railways-influence of various parameters. In: *IEEE International Symposium on Electromagnetic Compatibility (EMC)*, Detroit, MI, August 2008, pp.1–6. USA: IEEE.
11. Midya S, Bormann D, SchuüTte T, et al. DC component from pantograph arcing in AC traction system—Influencing parameters, impact, and mitigation techniques. *IEEE Trans Electromagn C* 2011; 53: 18–27.
12. Wang B, Wu G, Zhou L, et al. Pantograph arc's energy characters under various load. In: *IEEE 57th Holm Conference on Electrical Contacts (Holm)*, Minneapolis, MN, September 2011, pp.1–5. USA: IEEE.
13. Dong A, Wu G, Gao G, et al. Simulation system of pantograph arcing. In: *IEEE 2011 1st International Conference on Electric Power Equipment-Switching Technology (ICEPE-ST)*, Xi'an, People's Republic of China, October 2011, pp.637–641. USA: IEEE.
14. Wang W, Wu G, Gao G, et al. Experimental study of electrical characteristics on pantograph arcing. In: *IEEE 2011 1st International Conference on Electric Power Equipment-Switching Technology (ICEPE-ST)*, Xi'an, People's Republic of China, October 2011, pp.602–607. USA: IEEE.
15. Shea J and Zhou X. Contact material and arc current effect on post-current zero contact surface temperature. *IEEE Trans Compon Packag Technol* 2006; 29: 286–293.
16. Kuo MT and Lo WY. Magnetic components used in the train pantograph to reduce the arcing phenomena. *IEEE Trans Ind Appl* 2014; 50: 2891–2899.
17. Wang J, Yang Z, Lin F, et al. Analysis of electromagnetic characteristics of the main transformer caused by pantograph-catenary disconnection in high speed train. *Int J Eng Syst Model Sim* 2014; 6(1–2): 91–106.

18. Guardado JL, Maximov SG, Melgoza E, et al. An improved arc model before current zero based on the combined Mayr and Cassie arc models. *IEEE Trans Power Deliver* 2005; 20: 138–142.

19. Orlandi A. On the inclusion of switch arc restrikes and lossy ground in EMI analysis for HV substations. In: *IET Ninth International Conference on Electromagnetic Compatibility,* Manchester, UK September 1994, pp.92–98. UK: IET.

20. Cong H, Li Q, Xing J, et al. Modeling study of the secondary arc with stochastic initial positions caused by the primary arc. *IEEE Trans Plasma Sci* 2015; 43: 2046–2053.

21. Tseng KJ, Wang Y and Vilathgamuwa DM. An experimentally verified hybrid Cassie-Mayr electric arc model for power electronics simulations. *IEEE Trans Power Electr* 1997; 12: 429–436.

22. Thomas DWP, Pereira ET, Christopoulos C, et al. The simulation of circuit breaker switching using a composite Cassie-modified Mayr model. *IEEE Trans Power Deliver* 1995; 10: 1829–1835.

23. Bizjak G and Povh D. Circuit breaker model for digital simulation based on Mayr's and Cassie's differential arc equations. *IEEE Trans Power Deliver* 1995; 10: 1310–1315.

24. Tseng KJ and Wang Y. Dynamic electric arc model for electronic circuit simulation. *Electron Lett* 1996; 32: 705–707.

25. Tseng KJ, Wang Y and Vilathgamuwa DM. Development of a dynamic model of electric arc for power electronics simulations. In: *IEEE Industry Applications Conference, Thirty-First IAS Annual Meeting* (IAS'96), San Diego, CA, October 1996, vol. 4, pp.2173–2180. USA: IEEE.

26. Dai J, Hao R, You X, et al. Modeling of plasma arc for the high power arc heater in MATLAB. In: *The 5th IEEE Conference on Industrial Electronics and Applications (ICIEA)*, Taichung, Taiwan, June 2010, pp.463–468. USA: IEEE.

27. Rashtchi V, Lotfi A and Mousavi A. Identification of KEMA arc model parameters in high voltage circuit breaker by using of genetic algorithm. In: *IEEE 2nd International Power and Energy Conference (PECon)*, Johor Bahru, Malaysia, December 2008, pp.1515–1517. USA: IEEE.

28. Shaoping H, Qing Y and Jing L. Simulation of arc models based on MATLAB. *Proc CSU-EPSA* 2005; 17: 64–66.

29. Dai J. A Plasma arc model used in high power arc heater. *Trans China Electrotech Soc* 2011; 26: 129–134.

30. Suh Y, Lee Y, Kheir J, et al. A study on medium voltage power conversion system for plasma torch. In: *IEEE Power Electronics Specialists Conference (PESC)*, Rhodes, Greece, June 2008, pp.437–443. USA: IEEE.